PAPER • OPEN ACCESS

Low power consumption mini rotary actuator with SMA wires

View the article online for updates and enhancements.

Low power consumption mini rotary actuator with SMA wires

Luigi Manfredi, Yu Huan and Alfred Cuschieri

Institute for Medical Science and Technology (IMSaT), University of Dundee, Wilson House, 1 Wurzburg Loan, Dundee Medipark, Dundee DD2 1FD, United Kingdom

E-mail: mail@luigimanfredi.com

CrossMark

Abstract

Shape memory alloys (SMAs) are smart materials widely used as actuators for their high power to weight ratio despite their well-known low energy efficiency and limited mechanical bandwidth. For robotic applications, SMAs exhibit limitations due to high power consumption and limited stroke, varying from 4% to 7% of the total length. Hysteresis, during the contraction and extension cycle, requires a complex control algorithm. On the positive side, the small size and low weight are eminently suited for the design of mini actuators for robotic platforms. This paper describes the design and construction of a light weight and low power consuming mini rotary actuator with on-board contact-less position and force sensors. The design is specifically intended to reduce (i) energy consumption, (ii) dimensions of the sensory system, and (iii) provide a simple control without any need for SMA characterisation. The torque produced is controlled by on-board force sensors. Experiments were performed to investigate the energy consumption and performance (step and sinusoidal angle profiles with a frequency varying from 0.5 to 10 Hz and maximal amplitude of 15°). We describe a transient capacitor effect related to the SMA wires during the sinusoidal profile when the active SMA wire is powered and the antagonist one switched-off, resulting in a transient current time varying from 300 to 400 ms.

(Some figures may appear in colour only in the online journal)

1. Introduction

The design of a mini robotic system with several degrees of freedom (DOFs), is challenging mainly for the choice of the mini actuators. The challenge is exacerbated when the number of DOFs become high, i.e. in hyper-redundant robots. These can be designed by using external actuators (i.e. DC motors) and cables or tubes to transmit the motion [1–3]. An alternative solution is the use of internal (embedded) actuators to provide multiple DOFs. The advantages of external actuators design includes low weight and high force to weight ratio. However, with this design the number of DOFs is limited by the number of cables/tubes required [1–8]. The alternative

design based on internal actuators has two distinct advantages: it enables both modularity and multiple DOFs. The downside is increase in size and weight of the robot.

Another important requirement in the design of a robotics actuator is the control of the output force/torque for safe interaction with the surrounding environment, considered a challenge when the size of the robot becomes small.

1.1. Variable stiffness and impedance actuators

Actuators that can control the output force/torque are classified as variable stiffness actuators (VSAs) or variable impedance actuators (VIAs), depending on whether the controlled variable is either stiffness or impedance. In both, VSA and VIA, the position can be changed by an external force.

Biomedical applications for these actuators include surgery [9–12], rehabilitation, exoskeletons and humanoid robots, where

Figure 1. Low power consumption and light weight (0.7 g without the cover) mini rotary actuator (MiRA) with on board contact-less position and force sensors with overall measurements of $25.0 \times 9.0 \times 3.5$ mm.

safe interaction with humans and organs/tissues without collateral damage is crucial [13, 14].

Compliance can be active or passive, the former being achieved through an active control of the output impedance/stiffness with use of rigid actuators. Force/torque sensors, included in the control loop, ensure precise control of the compliance. However, because energy is consumed in the process, the overall efficiency of active compliance is low [15].

Passive compliance is achieved by incorporating compliant elements between the actuator and its output (e.g. springs), although this is limited because the compliance cannot be changed and is designed for a dedicated specific task. Moreover, it requires a minimum of two actuators for adjusting the compliance. In the antagonistic configuration, the two actuators are connected to the output link by two nonlinear springs. The most conventional set up uses tension springs and wires, functioning like human muscles. Other configurations have also been explored. Thus Torrealba and Udelman [16] reported on use of a cam running over a nonlinear profile to change the pre-stress on a nonlinear spring. Another study [17] reported a VSA created only from linear springs; whereas Guo *et al* [18] proposed four types of VSAs based on spring pretension with use of many parallel springs set at different angles. With this system, variable stiffness is achieved by adjusting the end points of the springs.

Unlike the antagonistic configuration, it is also possible to use one actuator for output control, while another one (usually smaller) to adjust the stiffness. The second actuator adjusts the stiffness by changing the transmission-ratio or transmission-angle, controlling the pre-stress on a nonlinear spring or the physical stiffness properties [19, 20]; as advantage, the output torque is not influenced. Jeong *et al* [21] reported on the use of two-worm gear transmission to compress two coiled springs and change their output stiffness. In continuum robotics with wire transmission, increasing tension in the wires is used to increase stiffness [11, 22]. More recently, several designs have been proposed in which

vacuum is used to increase stiffness by compressing layers, implementing on-off modes [9, 10]. Ranzani *et al* [12] propose a modular joint rather than a continuum manipulator, where the stiffness of each individual joint can be adjusted by applying vacuum to its central channel filled with granular-jamming-based stiffening mechanism.

1.2. Shape memory alloy (SMA) actuators

Minimal access surgery (MAS) imposes limitations on the overall size of a medical device, hence most VSA designs are too large or heavy for this approach. Prototypes of the above mentioned applications for MAS have been produced on a larger scale [9, 10]. In all of the reported designs, the size of the actuator is not suitable for being embedded in a robotic platform.

Smart materials, such as SMAs, can play a key role in reducing the size of the actuators due to the high force to weigh ratio achieved in a small size. Limitations of this smart material include its low energy efficiency, which varies from 5% to 7% [23], and limited stroke, up to 7% of their total length. This is a compromise between the range of motion and output torque for a rotary actuator, as discussed in section 3.2. Fatigue can limit the life of SMA wires as reported by several studies [24–26]. Additionally, SMA wires dynamic performance is related to the heat dissipation causing hysteresis. This can be an issue for the control implementation, which may require complex nonlinear algorithm and the need for SMA wire characterisation [27, 28].

Several configurations have been proposed for designing rotary actuators by having SMA wires in antagonistic configuration [29, 30]. Because an SMA wire can be contracted by heating and extended by applying an external force, the antagonistic configuration can be designed by using an SMA wire and a spring, or two SMA wires connected to a pulley to transmit the motion [31].

1.3. Mini rotary actuator (MiRA) actuator

The output torque of an actuator can be controlled by using force sensors in series with each SMA wire [32–34]. This design approach can limit the overall length and weight of a mini actuator, since the available off-the-shelf linear force sensors are not small enough in size.

To achieve both a compliant behaviour and a compact design, the authors in the present study constructed a rotary actuator by using SMA wire in antagonistic configuration and miniature pulleys to reduce the overall length, together with force and position sensors (figure 1). The two SMA wires are independently controlled to achieve a compliant behaviour by using embedded force sensors, thereby keeping the overall design small.

Analysis and experiments on the energy consumption show a very low power consumption required to keep a specified angle position (when no external forces are applied), and together with the mechanical bandwidth make this actuator suitable for a design of a mini robotic platform. The
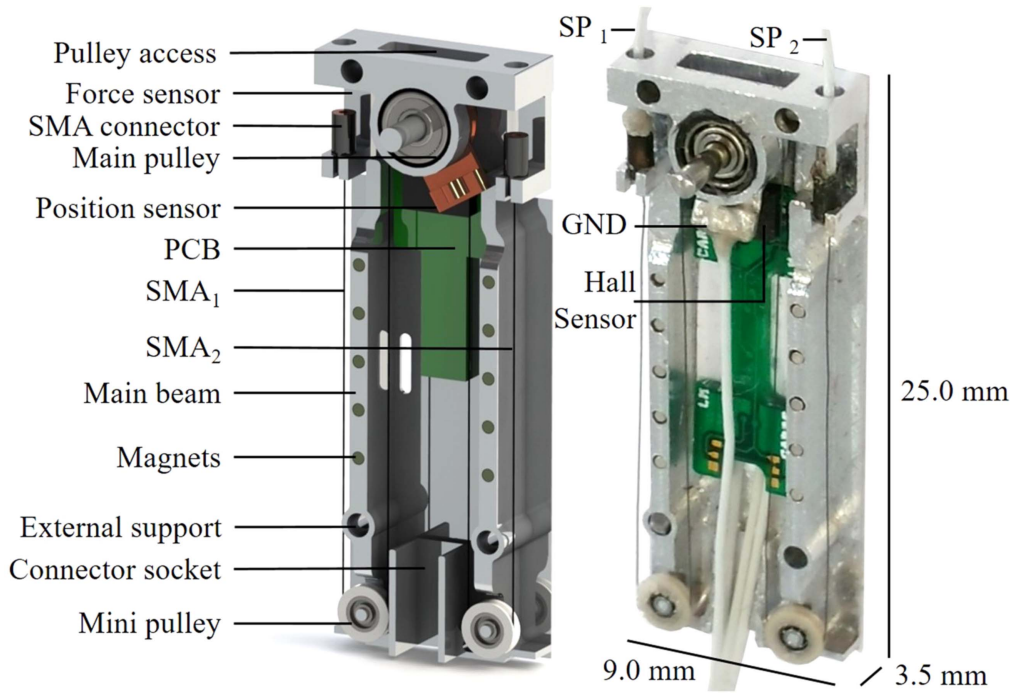
Figure 2. Actuator design using SMA wires in antagonistic configuration. Novel design of mini force and position sensors with on-board electronics to measure the angle of the main pulley and the torque produced.

presented work considerably extends the scope of the preliminary results reported previously by the authors [35].

2. Methods

MiRA is a mini rotary actuator with a low power consumption designed for being used in mini robots. It is composed of a light aluminium frame, a shaft connected to a main pulley rotated by two SMA wires in antagonistic configuration, which are controlled independently. The shaft angle and the output torque can be controlled by a purpose-designed set consisting of one position contact-less sensor, and one torque sensor. The overall length of the actuator is reduced by half by the use of two mini pulleys with miniature ball bearings, as shown in figure 2. The main pulley is connected to a shaft supported by two small ball bearings to reduce friction. Each SMA wire is powered independently by means of two electrical wire SP_1 and SP_2 (figure 2) and they are fixed to the main pulley by using conductive silver epoxy glue (Circuitworks® CW2400). An additional electrical wire connected to the may pulley, provides grounding between the two SMA wires and to power each of them independently. The basic MiRA designed can use SMA wires of different diameters, resulting in different output torques, mechanical bandwidth and energy consumption.

The design parameters are the output torque τ_{MAX} and the range of motion $2\alpha_{max}$ related to the diameter and total length of the SMA wires. The output torque affects the mechanical bandwidth, by which the thicker the wire, the higher the torque, and the lower the bandwidth.

In the design, the contraction of the SMA wires was estimated conservatively at 3%. Each SMA wire is fixed to a beam, which has a strain gauge (SG) glued on the back to measure the mechanical deformation and therefore the force produced.

The SGs have a half bridge configuration and were tested by using an Instron® 5564 dual columns. The SGs configuration was suitable to measure the output torque reducing the need of complex electronics for signal processing and providing the output torque as an indirect measurement by only a single analogue output value. The SGs wiring is simplified by being connected to a beam. As most of the torque sensors are included in the main pulley and rotate with the shaft, wiring is difficult because of the overall size of the main pulley (3.9 mm), limiting the available space for gluing the SGs. Our proposed solution avoids the wiring rotation issue and reduces the overall size of the main pulley.

The angle of the shaft is measured by using a contact-less position sensor with a hall effect chip and a permanent magnet to reduce any additional friction and increase the overall efficiency of the actuator.

Both position and torque sensors have been characterised and the performance represented graphically. The position sensor calibration shows a good linear profile and the torque sensor is reliable with good performance despite the small size.

Experiments have been performed by using an Arduino Leonardo board where a PID control implements a sinusoidal wave with different frequencies (i.e. from 0.5 up to 10 Hz) and different step profiles. The SMA wires have a diameter of 76 μm since they have shown a good mechanical bandwidth. The position tracking has been implemented by using a PID

controller without including the SMA wires model characterisation in the control loop. Energy consumption was assessed and confirmed to be low in maintain a selected angle position. No overheating issue has been observed, due to low power consumption and because the thermal conductive metal frame was used to dissipate any overheating.

The results of the experiments have demonstrated that MiRA is suitable for being adopted for mini robotic applications due to its mechanical bandwidth performance, the torque sensory feedback and, in particular, its negligible energy consumption to maintain any required position.

3. Actuator design

MiRA was conceived as a modular actuator with all the required components incorporated within, suitable for the design of hyper-redundant robots. It can be controlled by using the angle position α_r, maximal torque τ_{MAX}, and it can provide the actual position α and produced torque τ.

In the following sections, each component of MiRA is described in detail.

3.1. SMA wires in antagonistic configuration

Rotary actuators with SMA wires in antagonistic configuration can be designed by using the following configurations: (i) one SMA wire to actively rotate the actuator in one direction and one spring material to passively rotate it in the opposite direction by stretching the SMA wire; (ii) two SMA wires to actively rotate the actuator in both directions.

Configuration (i) is for applications where one desired position has to be kept without any energy consumption through the use of the spring material. When a desired angular position has to be maintained for long, the SMA wire needs to be powered to stretch the spring material, hence resulting in a high power consumption. Additionally, since the rotation in one direction is actively controlled by the SMA wire activation and the opposite direction passively controlled by the spring, the mechanical bandwidth is not symmetric, resulting in a limitation of the overall actuator performance.

Configuration (ii) uses two SMA wires, each controlling the rotations in either direction of the actuator by stretching the opposite one. This results in a symmetric performance in the control of the position and a better mechanical performance throughout the frequency range. The main advantage of this approach is the low power consumption when a required position needs to be kept for a long period. This advantage is related to the fact that when the desired angle position is achieved and no external torque is applied, only one SMA wire is active providing a negligible force to keep the opposite SMA wire stretched. As a result, the energy required to keep an arbitrary position is very low.

To reduce the overall length of the actuator, each SMA wire can be wound over a mini-pulley, produced bending

Table 1. Output performances with different SMA wires.

Diameter (μm)	Max. force (N)	Max. torque (N mm)	Max. micro-strain at force sensor
76	0.8	1.56	270
100	1.43	2.78	482
130	2.23	4.34	752
150	3.21	6.26	1083

strain described by the following equation:

$$\epsilon_{\max} = \frac{\frac{d}{2}}{R + \frac{d}{2}}, \qquad (1)$$

where $\epsilon_{\max}$ represents the maximal normal strain, R is the radius of the pulley, and d is the diameter of the SMA wire. Although additional mini-pulley can reduce the overall length of the actuator, this additional strain carries the risk of precipitating stress fatigue of the SMA wire [36].

For robotics applications, mechanical bandwidth and energy consumption are essential requirements for the choice of actuators. This is what has led us to design MiRA by choosing the configuration (ii), by using two SMA wires in antagonistic configuration.

3.2. Frame design

Details of SMA wires adopted for the design are shown in table 1, and were able to generate a force ranging from 0.8 to 3.21 N. To achieve high torque to weight ratio, the frame was designed to be as light as possible by using aluminium alloy, obtaining a weight of 0.52 g and outer dimensions of 25.0 × 9.0 × 3.5 mm (figure 2). The frame was designed by using finite element analysis (FEA) and stressing the structure with two forces of 5 N for each beam, above than the maximal force produced by the thicker SMA wire (150 μm of diameter), which is 3.21 N.

The structure is composed of two main beams supporting all the stress, connected together with the main pulley to the upper part as shown in figure 3(a). The back of the actuator is 0.1 mm thick and serves as a cover and support for the electronic board. The top part has a slot to provide access to the pulley. Four holes, two in the top part and two more in the bottom part, provide a connection to any external support.

The FEA was performed by applying forces as shown in figure 4. One force of $F_S = 5N$ is applied to each beam and one more force $2F_S = 10N$ is applied to the main pulley and to each pin where the small pulleys are connected. The stress force is concentrated in the two miniature bearing shafts in the bottom part of the design, because the diameter of the shaft being only 0.5 mm. The FEA (figure 4) confirmed that the stress is below the Yield strength (aluminium alloys, 7050, Yield strength 4.70×10^8 N m^{-2}), therefore able to sustain these forces.

The SMA wires are fixed to two small rectangular beams (0.3 × 1.2 mm), connected only with the upper side to the main frame, free to move and designed to function as force
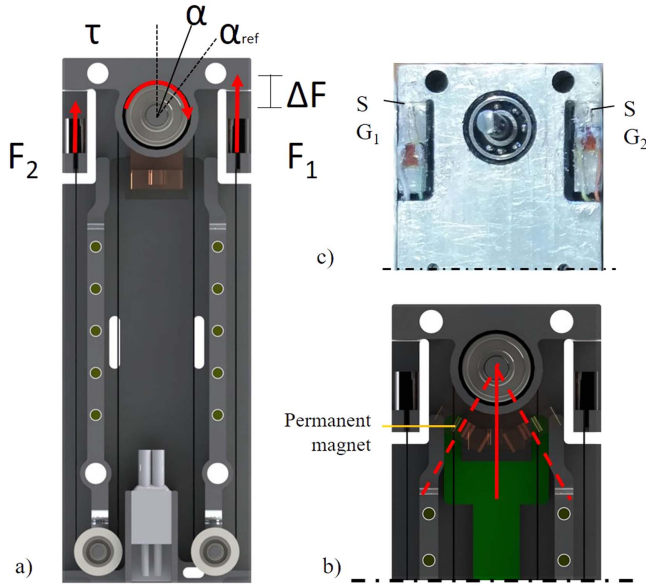
Figure 3. (a) The MiRA's working principle, where F_1 and F_2 are the two forces produced by each SMA wire and measured by the force sensors. α_{ref} is the reference angle for the position control and α is the actual angle measured by the contact-less position sensor. (b) Position sensor in three configurations: $-\alpha_{MAX}$, $0°$, α_{MAX}. A miniaturised permanent magnet is located beneath the main pulley. (c) Semiconductor strain gages glued on the back side of each beam.

sensors. They exhibit a deformation over 1000 micro-strain, when a force of 3.21 N is applied. The rectangular cross section of the beams ensures a lower inertia in the direction of the stress and higher in other directions.

The main pulley and the small pulleys have a ball bearing to reduce friction, which is essential for the overall actuator performance, avoiding any stick-slip issue in the control architecture. The main pulley holds the shaft and is connected to the main frame by means of two ball bearings with an overall size of $1.0 \times 1.0 \times 3.0$ mm. The small pulleys use miniaturised ball bearing measuring $0.5 \times 0.8 \times 1.5$ mm, produced by Minebea.

The design of the main pulley diameter is a compromise of the output torque τ_{MAX}, the angle range of motion $2\alpha_{MAX}$, and the overall length of the actuator, as described by the following equations:

$$\tau_{MAX} = r_P F_{MAX}, \tag{2}$$

$$l_S = 2l_A, \tag{3}$$

$$l_R = l_S \epsilon = 2l_A \epsilon, \tag{4}$$

$$\alpha_{MAX} = \frac{l_R}{r_P} = \frac{2l_A \epsilon}{r_P}, \tag{5}$$

where $r_P = 1.95$ mm is the radius of the main pulleys, F_{MAX} is the difference between the force produced by the activated SMA wire and the force needed to stretch the opposite one, l_A is the distance between the main pulley and the small pulley, $\epsilon = 3\%$ is a precautionary contraction percent, l_S is the total length of one side SMA wire, and l_R the overall contraction of the SMA wire.

3.3. Position sensor design

Off-the-shelf position sensors for such a small actuator are resistive, and composed of two plates, one fixed to the frame, and the other moving with the shaft. The rotation of the movable plate produces variation in the output resistance, providing an analogue information of the absolute position. Advantage of this sensor is the small size and information of a whole 360° turn. The limitation is that the two plates need to touch each other, producing friction and therefore a resistive torque, which has to be overcome by the actuator and results in a reduction of a total output torque. The smallest available are the muRata SVM4 Series [37], with an overall size of $4.0 \times 4.5 \times 2.0$ mm and a resistive maximal torque of 6 N mm, which is almost the maximal output torque produced by MiRA.

An contact-less position sensor was designed to avoid any friction and reduction in the output torque. The sensor consists of a hall effect chip fixed into the electronic board in the main frame to measure the magnetic field produced by a small permanent magnet located in the main pulley and rotating with the shaft (figure 3). Limitations of this approach are the maximal angle measured, which in this design cannot exceed 180° due to the symmetry of the magnetic field, and the output position profile being highly nonlinear when the angle is close to the limit range of $\pm 90°$. In MiRA design the range of motion is less than this limit, making this design suitable in terms of linear response, and a better choice compared to the commercial available sensors in terms of resistive torque and overall dimension. The mechanical range performed by the actuator is shown in figure 3(b).

The novel design permits the actuator to be more compact and the sensor to be integrated into the structure. The output is acquired by using an analogue to digital converter (A/D) with a resolution of 10 bits. The power consumption is less than 0.5 mW at 3.3 V, and the voltage output spread from 150 (0.48 V) to 450 (1.45 V) digital value, for a total angle range of $\pm 15°$. The relation between the analogue output digitalised by the A/D converter, and the measured angle is reported in figure 5(a), where is shown a linear performance in throughout the working range. The resolution expressed in degrees per bit ($°\,bit^{-1}$) is described by the following equation:

$$\Delta V = V_{MAXL} - V_{MINL}, \tag{6}$$

$$\Delta V_B = \frac{\Delta V}{V_P} 2^{AD}, \tag{7}$$

$$\alpha_B = \frac{2\alpha_L}{\Delta V_B}, \tag{8}$$

$$\alpha_B = \frac{30°}{(450 - 150)\,bit} = \frac{30°}{300\,bit} = 0.1°\,bit^{-1}, \tag{9}$$

where, V_{MAXL} and V_{MINL} are the higher and lower digital voltage, $AD = 10$ the resolution, V_P the power of the A/D converter, and α_B is minimum angle per bit measured.
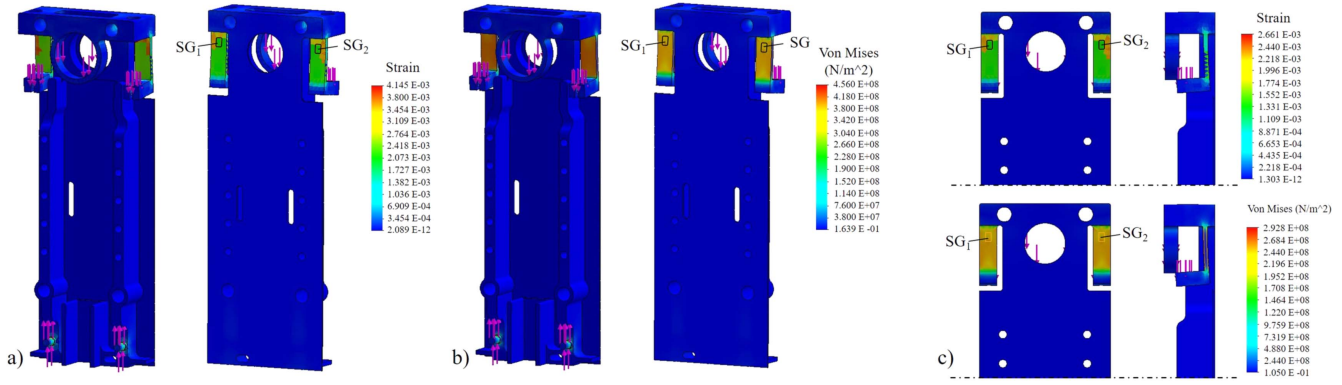
Figure 4. Finite element analysis (FEA) of the strain of the structure (a), and stress (b), with front view (a) and back view (b) of MiRA. A force of 5 N has been applied on each beam, as represented by arrows in the picture. The frame is made of aluminium alloys 7050, with a yield strength of 4.70 $\times$ 10^8 N m^{-2}. (c) FEA of the beam strain with front (left), lateral (right), front (top) and back view (bottom) of MiRA with the real deformation. Force of 3.21 N is applied to each beam, and a force of 6.42 N to the main pulley and to the two small ball bearing shafts. These forces can be produced by two SMA wires with a thickness of 150 μm.

3.4. Torque sensor design

Conventional torque sensors are designed to be connected to the shaft of the transmission by using different measurement methods, such as magnetic [38–40], capacitive [41], MEMS [42], or SGs. SGs are commonly used for this application, by measuring the deformation and relating this to the input torque. SGs can be resistive [43–45], with a limited gauge factor (GF) of less than 2, or semiconductor, with a GF up to 170 [46]. Resistive SGs need a signal processing circuit (i.e. Wheatstone bridge) and a signal amplifier to reduce the temperature drift and to achieve a wider output range. Semiconductor SGs, due to a high GF, can be processed without an amplifier, since the output range is much higher than the resistive one. Semiconductor and resistive SGs both have temperature drift but in the semiconductor one the GF is more relevant, which requires a measurement of the temperature to compensate this effect and to improve the measurement accuracy.

In MiRA, a torsional torque sensor cannot be embedded in the pulley because of the limited available space. This raises two issues: (i) difficulty in locating and gluing the SGs; (ii) the electrical wiring will move with the pulley, causing an issue with the cabling.

In the proposed design, because the pulley is moved by using SMA wires, the torque produced by the actuator can be calculated by measuring the force produced by each wire [47].

In contrast to the previous state of the art, and due to a limited available space, sensors have been embedded into the frame structure. The torque generated by MiRA is obtained by measuring the difference between the force provided by each SMA wire, multiplied by the radius of the pulley as shown in figure 3(b) and described by the following equation:

$$\tau = R_{\mathrm{P}}(F_1 - F_2) = R_{\mathrm{P}}\Delta F, \tag{10}$$

where R_{P} is the main pulleys radius, which is 1.95 mm, and F_1 and F_2 are the forces produced by the two SMA wires to the main pulley, and measured by the two force sensors.

Each beam has been designed to work as a sensor by using a semi-conductor SG glued on the back side as shown in figure 3(c). The SG are produced by micron instruments [48] model number SS-018-011-3000PU, with an overall size of 4.57 $\times$ 3.04 $\times$ 0.01 mm, GF = 100 $\pm$ 10, and a resistance of 3000 $\pm$ 150 Ω at 25 °C

SGs can be connected by using different configurations as shown in figure 6. The one selected for MiRA, is the (c) solution, because it simplifies the cabling and has only one analogue output value to measure. The pros and cons of the other configurations are reported in the appendix. Output voltage in relation with the input force, is described by the following equation:

$$V = 1 - \frac{1}{2 + \frac{\Delta R_F}{R_0 + R_{F1}}}, \tag{11}$$

where $\Delta R_F = R_{F2} - R_{F1}$, and R_{Fi} represents the resistance variation produced by the force F_i and described in detail in the appendix.

The proposed SG configuration compensates for the temperature drift but the GF temperature effect remains and contributes to the overall error. This can only be compensated by using a dummy SG as a temperature sensor, one for each beam, in order to precisely measure the force produced by each SMA wire. For compensation of the GF temperature effect, the electronic hardware needs to incorporate four A/D converters in total, two for each SG and two for the dummy SGs. This will require two additional SGs, aside from the requirement for more wires, making the cabling even more challenging.

An important consideration is that in such small size, most of the actuators do not have any force feedback, therefore its inclusion can be considered a great improvement.

To reduce the number of electronic components the signal is sent to an AD converter with 24 bits of resolution and due to the high GF no amplifier is needed to achieve a high resolution.
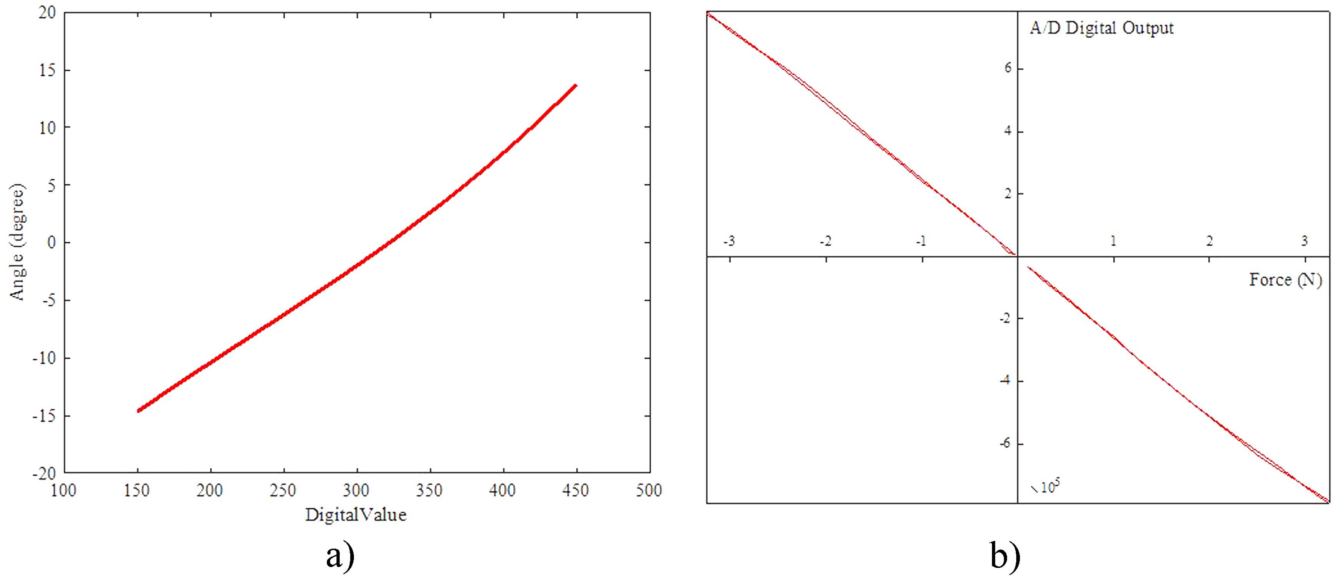
a)

b)

Figure 5. (a) Graph of α in degrees versus the digital value acquired by the bridge board. (b) SGs calibration by using an Instron®. Graph of the applied force versus the digital output read by the A/D converter. The experiments were performed by applying a force to each beam of the actuator and repeating the test 5 times for each beam.
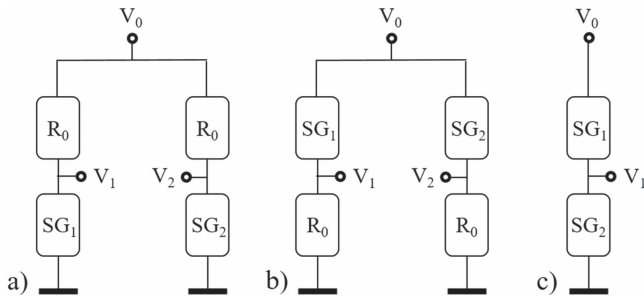

Figure 6. A voltage driver measures the output provided by each strain gage in three configurations, (a) the one chosen to have a wider output range, (b) an alternative solution with lower range and the solution (c) can use only one A/D converter instead of two like the solution (a) and (b).

Each force sensor was designed to achieve up to 1120 micro-strain when a force of 3.3 N is applied by each SMA wire. Table 1 reports the SMA wires performance considered for the actuator. The micro-strain in the table corresponds to the strain for the maximum force of the specified SMA wire at the location of the SGs.

Each force sensor has been tested by using an Instron® 5564, and applying a force from 0 to 3.25 N to each beam. The instrument was programmed to perform 5 cycles for each step, consisting in applying and releasing the force in each of the steps. The force was increased by 0.25 N at the end of each cycle. The digital output for each trial was acquired and the average value reported in the graph by showing in the *X* axis the applied force and in the *Y* axis the digital output. The sensor performance has confirmed good linearity and repeatability even in such small dimension as shown in figure 5(b). High sensitivity, less than 0.1 N of resolution, and low noise have been observed during the experiments.

4. Result and discussion

Experiments have been focused to investigate the energy consumption through the implemented sinusoidal waves and step angular profiles in the absence of any external load being applied. This was necessary to determine the energy required to maintain a desired position during the energy is absorbed only by the SMA wires. Additionally, the output torque was measured.

All the experiments were performed at room temperature and by using standard Flexinol® actuator SMA wires produced by Dynalloy® Inc., with a prestrain of about 2%.

4.1. Energy consumption

Sensors (3513 0—CE-IZ02-32MS2-0.5 DC 0–1 A) where used to monitor the current in both SMA wires. Each SMA wire was controlled by a pulse width modulation (PWM) provided by an Arduino Leonardo and an Arduino Motor Shield, powered by a current limited to 200 mA at 5 V. The PID controller was implemented in Arduino in real-time. All the data acquired from Arduino, i.e. angle position control profile and the one provided by the angular sensors, PWM and current for both SMA wires, were sent via a serial communication interface to Matlab® Simulink.

Sinusoidal and step position profiles were tested without any external torque with use of SMA wires of 76 μm diameter, as shown in table 1. This gauge of wire was selected based on data from preliminary experiments indicated that it exhibited a good compromise between mechanical bandwidth, output torque and energy consumption.

Figure 7(a) shows a sinusoidal position $A_0 \sin(2\pi f_0 t)$ profile with a 76 μm SMA wires, and with the following frequency and amplitude (f_0, A_0): {(1 Hz, 15°), (1.5 Hz, 15°), (2.5 Hz, 10°)}. The position control was
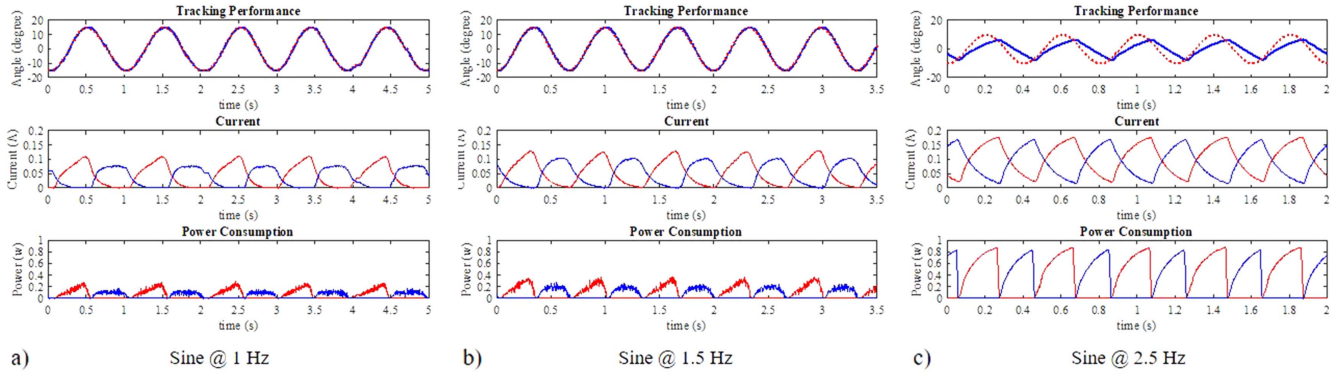
Figure 7. Graph profiles of the sinusoidal angular position control at 1, 1.5 and 2.5 Hz where is showing (a) α position, (b) current and (c) power of each SMA wire.
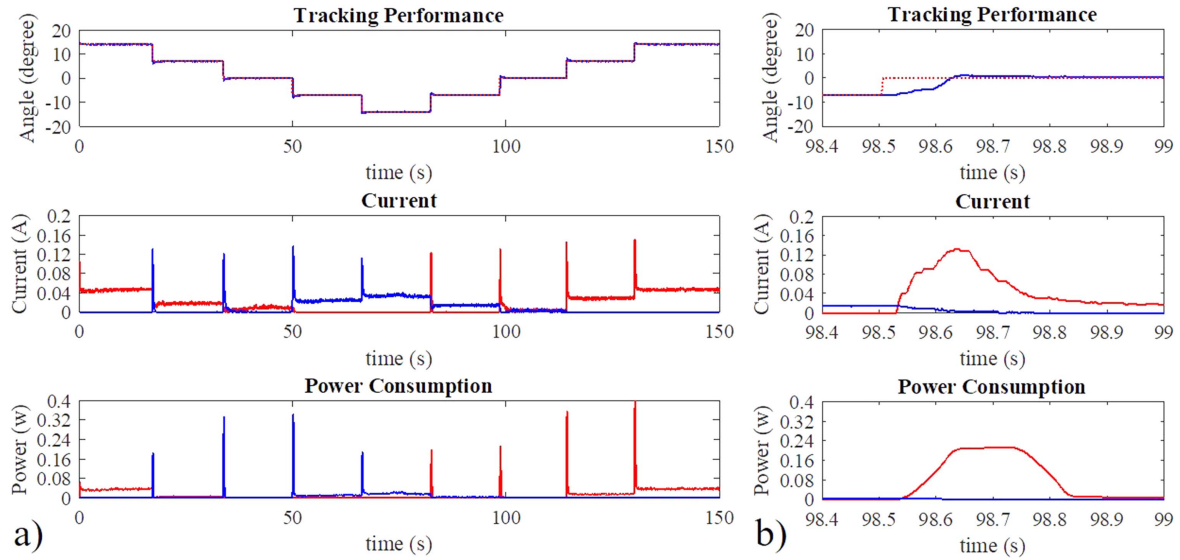

Figure 8. (a) Step profile from $-15°$ to $15°$, with a step of $7.5°$; the power consumption has a transient peak and then become negligible, less than 0.04W. (b) A step response of $7.5°$ shows a time delay of only 120 ms and a peak power of 0.22 W.

implemented by using a PID control and the graphs showed the expected response.

When the frequency increases the range of motion of the sinusoidal wave becomes smaller due to the limitation in the mechanical band-width. The position tracking shows a good performance for a range of $\pm15°$, at frequencies f_0 of 1 and 1.5 Hz, with a power consumption below 140 mW. The energy also increases with power consumption below 900 mW for a frequency $f_0 = 2.5$ Hz and amplitude $A_0 = 10°$. The performance is related to the diameter of the wire, and the diameter of the pulley, which in turn is directly proportional to the output torque, and indirectly proportional to the range of motion. The diameter of the pulley affects the overall length of the joint, because of its relation with the range of motion. Additionally, the energy consumption is related to the length of the wire, as described by the following equation:

$$P = RI^2 = \rho\frac{l}{d}I^2,\qquad(12)$$

where R is the resistance, ρ the electrical resistivity, d the diameter and l the total length of the SMA.

Figure 8 shows a step profile with different angles $\alpha_r = (-15°, 0, 15°)$, where the step from $-7.5°$ to $0°$ is zoomed in figure 8(b). In this configuration, the output torque and power, are both at peak at the start of the position control and become negligible when the desired position is achieved. This peak is due to the mechanical resistance provided by the opposing SMA wire, resulting in a higher power consumption and in a reduction of the output available torque. The situation would be different with adoption of antagonistic spring instead of an SMA wire since the force provided by a spring would keep the energy consumption constantly high, reducing output torque and exhibiting a asymmetric behaviour. This increase in the energy consumption is only transient, confirming good energy efficiency performance by the twin SMA wires antagonistic configuration design, compared to a single SMA wire and spring combination. Advantage of this short transient power peak (about 300 ms) results in a higher output torque by the actuator, since there is no opposite force produced by the antagonistic SMA wire.

Figure 9 shows the sinusoidal amplitude versus frequency reaching a maximal frequency of 10 Hz. The
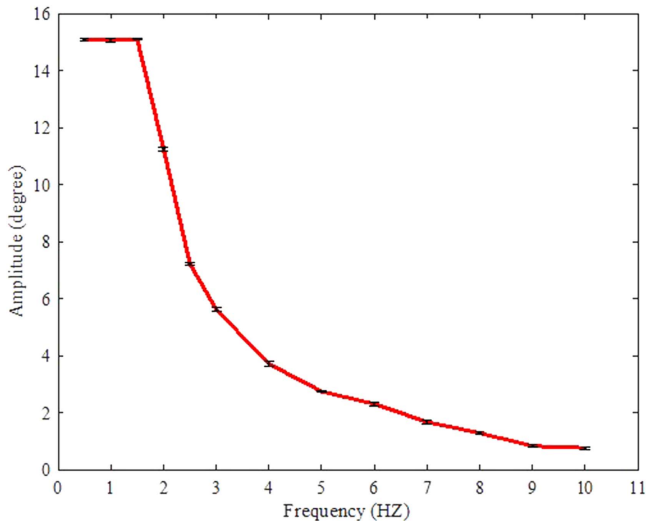
Figure 9. Sinusoidal amplitude versus frequency graph. The sinusoidal wave amplitude decreases starting from 15° at 0.5 Hz up to 0.8° at 10 Hz. The reported data were acquired performing the experiment twice for each frequency and measuring the average value and standard deviation of a sinusoidal wave for 5 cycles and two trials each.

limitation in the amplitude with higher frequency is obviously related to the mechanical bandwidth of the actuator due to the heating.

Both figures, figures 7 and 8, report a transient current in the opposite SMA wire when powered-off. It is evident that the power consumption is zero and the current is decreasing towards zero with a transient phase varying from about 400 ms for a sinusoidal wave at 1 Hz, and up to about 300 ms for a sinusoidal wave at 2 Hz. This behaviour is mainly related to a capacitor-like effect of the SMA wire, which releases the stored energy from by the previous activation when is stretched by the opposite SMA wire. Part of this behaviour is contributed by the capacitors in the driving circuit though considered of a second order when compared to the SMA capacitor-like effect. Reducing this transient time can increase the mechanical bandwidth.

4.2. Produced torque

The output torque was measured by connecting an additional external pulley (10 mm diameter) to the shaft of the actuator. For the measurement of the produced force and hence torque, a cable was used to connect the external pulley to the Instron® and consequently the output torque (figure 10(a)). The torque was measured by imposing an angle position of $\alpha_m = -15°$ to the MiRA PID controller, and pulling the cable by a step profile preprogrammed into the Instron® up to an angle of $\alpha_M = +15°$, in a quasi-static configuration.

The torque versus angle is almost linear as illustrated in figure 10(b). When the angle is close to the lower limit $(-15°)$, the output torque is equal to 0 N mm because the activated SMA wire is fully contracted. The torque is maximal when the angle is close to the upper limit $(+15°)$, when the SMA wire is fully stretched.

5. Conclusion

This paper reports the design of MiRA, a mini rotary actuator based on using SMA wires in antagonistic configuration. Miniaturised pulleys are deployed to reduce the overall length of the actuator and miniature ball bearings to minimise friction, thereby increasing the overall efficiency of the system. A mini contact-less position sensor was designed to measure the output angle. The output torque is calculated by measuring the deformation of two beams with SGs, to which the SMA wires are connected. Both sensors have been tested and calibrated in a closed loop control. The mechanical design is described in detail and the results of experiments, performed by using a sinusoidal angular profile, are reported and discussed. Negligible energy consumption to keep a desired angular and fast response was reported for a step angular profile and a sinusoidal wave up to 10.0 Hz.

The compact size, low energy consumption and the modularity of the design, makes this actuator suitable for construction of hyper-redundant light and miniature robots exemplified by MiRA. The hardware has been shown to be robust and the sensory systems provide the possibility for further investigation of position and impedance control. Additional improvements are needed in terms of control and electronic hardware design, including on-board control hardware which now includes only a hall chip sensor for the measurement of the position angle. The design of MiRA includes a central rectangular space, which is sufficient to accommodate embedded electronic board and other components required to construct a servo motor.

Further experiments are needed to investigate the capacitor-like effect, which can be included in the control algorithm and in the driver hardware to reduce the transient current. This includes an analytic model of this phenomenon not previously reported to the authors knowledge.

The environmental temperature can effect the actuator performance in terms of energy consumption and mechanical bandwidth. In all the experiments MiRA has not shown an variations in the overall performance and reliability of the actuator. The PID parameters have not needed any changes after the first calibration process.

Specific fatigue tests have not been performed although we have not had any issue with any SMA wire, even after a prolonged time of experiments. No issues have been reported in the more stressed section of the SMA wires, which is the one next to the mini-pulleys for the additional stress, as described in detail in the section 3.1. We plan to investigate the fatigue performance in future works.
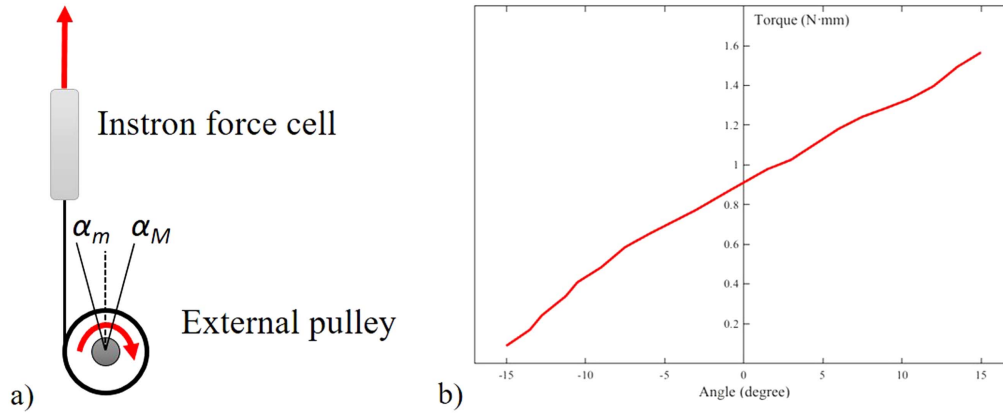
Acknowledgments

Figure 10. The output torque experiment set-up is shown in figure (a), and the graph torque versus angle is shown in figure (b).

Appendix

The SGs values can be measured by using three different solutions as showed in figure 6, resulting in different output errors and number of required wires for cabling each SG. The GF temperature effect is not considered because to cancel this error additional temperature sensors need to be located close to each SG. Each configuration will be described in detail in the following sub-sections.

Configuration (a)

In this subsection we describe the voltage driver adopted for the signal acquisition shown in figure 6(a) where the SG is connect to the bottom part of the bridge.

The force measured by each SG is described by the following equations:

$$V_i = V_0 \frac{R_{Gi}}{R_0 + R_{Gi}}, \tag{13}$$

where R_0 is chosen according to the strain gage resistance at 25 °C, V_i, with $i = 1, 2$, is the voltage measured by each A/D converter and R_{Gi} the resistance provided by each SG. This is not a conventional method to acquire SGs due to several errors included in the measurement discussed in detail below.

In all the following discussion, we assume that R_0 temperature effect is negligible if compared with other errors included in the acquisition process. This can be considered a valid hypothesis if the resistors have a low temperature coefficient of resistance. Each strain gage's resistance change as follows:

$$R_{Gi} = R_0 + R_{Fi}, \tag{14}$$

where R_{Fi} represent the resistance variation provided by the applied force and the equation (13) become as follows:

$$V_i = V_0 \frac{R_0 + R_{Fi}}{R_0 + R_0 + R_{Fi}} = V_0 \frac{R_0 + R_{Fi}}{2R_0 + R_{Fi}} \tag{15}$$

which represents each force produced by each SMA wire. By using the equation (10), we can assume that the output torque

is proportional to the different of voltage $V_2 - V_1$:

$$\Delta V = V_2 - V_1 = V_0 \left(\frac{R_0 + R_{F2}}{2R_0 + R_{F2}} - \frac{R_0 + R_{F1}}{2R_0 + R_{F1}} \right) \tag{16}$$

$$= V_0 \frac{R_0 R_{F1} + 2R_0 R_{F2} - R_0 R_{F2} - 2R_0 R_{F1}}{4R_0^2 + 2R_0 R_{F1} + 2R_0 R_{F2} + R_{F1} R_{F2}} \tag{17}$$

$$= V_0 \frac{R_{F1} + 2R_{F2} - R_{F2} - 2R_{F1}}{4R_0 + 2R_{F1} + 2R_{F2} + R_{F1} R_{F2}/R_0} \tag{18}$$

$$= V_0 \frac{R_{F2} - R_{F1}}{4R_0 + 2(R_{F1} + R_{F2}) + R_{F1} R_{F2}/R_0}. \tag{19}$$

Equation (19) describes the relation between the output measured voltage ΔV and the output torque, $\tau = f(\Delta V)$. Considering $R_0 \gg R_{F1}$ and $R_0 \gg R_{F2}$ due to mechanical property of SGs, we can assume the following statement:

$$4R_0 \gg 2(R_{F2} + R_{F1}) + \frac{R_{F1} R_{F2}}{R_0}. \tag{20}$$

Equation (19) become as following:

$$\Delta V_a = V_0 \frac{(R_{F2} - R_{F1})}{4R_0}, \tag{21}$$

where $\Delta V_a \approx \Delta V$.

The output torque is proportional to the $R_{F2} - R_{F1}$:

$$\Delta R_F = R_{F2} - R_{F1} \tag{22}$$

therefore the output torque is related to the following equation:

$$\tau = f(\Delta R_F) \tag{23}$$

and ΔV_a become as following:

$$\Delta V_a = f_V(\tau). \tag{24}$$

The equation (21) represents an error in the measurement which is considered acceptable if we want to reduce the size of MiRA and make it so small. From equation (20), this error is maximal when $R_{F2} \approx R_{F1}$ and the equation $\Delta V \approx 0$, therefore this condition is not considered as a risk, since the output torque is almost 0. The risk condition occurs when the output torque is higher, therefore, either $R_{F1} = 0$ or $R_{F2} = 0$.

Assuming $R_{F1} = 0$, the equation (19) become as following:

$$\Delta V = V_0 \frac{R_{F2}}{(4R_0 + 2R_{F2})} \qquad (25)$$

and by using the previous approximation we obtain the following equation:

$$\Delta V_a = V_0 \frac{R_{F2}}{4R_0}. \qquad (26)$$

The error in the measurement is represented by the following equation:

$$e = \frac{\Delta V - \Delta V_a}{\Delta V} = 1 - \frac{\Delta V_a}{\Delta V} \qquad (27)$$

and by using equations (25) and (26), the error is as following:

$$e = 1 - \frac{4R_0 + R_{F2}}{4R_0} = -\frac{R_{F2}}{4R_0}. \qquad (28)$$

Considering that $R_{F2} = GR_0$, where G is the ration between R_{F2} and R_0, which is not more than 0.1 (empirical value obtained by out experiments), the error become as following:

$$|e| = |\frac{GR_0}{4R_0}| = |\frac{G}{4}| \qquad (29)$$

obtaining 0.025, therefore 2.5% as maximal error.

Configuration (b)

The solution shown in figure 6(b), proposed to swap R_0 and R_{Fi} and obtaining the following voltage driver equations:

$$V_i = V_0 \frac{R_0}{R_0 + R_{Gi}}, \qquad (30)$$

where, R_0 is chosen according to the strain gage resistance at 25 °C, V_i, with $i = 1, 2$, are the voltage measured by each A/D converter. Each strain gage's resistance change as follows:

$$R_i = R_0 + R_{Fi}, \qquad (31)$$

where $R_{Fi} = R_0 + G_i F_i = R_0 + R_{Fi}$ represent the resistance variation provided by the applied force and the equation (31) become as follows:

$$V_i = V_0 \frac{R_0}{R_0 + R_0 + R_{Fi}} = V_0 \frac{R_0}{2R_0 + R_{Fi}} \qquad (32)$$

which represents each force produced by each SMA wire. By using the equation (10), we can assume that the output torque is proportional to the different of voltage $V_2 - V_1$:

$$\Delta V = V_2 - V_1 = V_0 \left(\frac{R_0}{2R_0 + R_{F2}} - \frac{R_0}{2R_0 + R_{F1}} \right), \qquad (33)$$

$$\Delta V = V_0 \left(\frac{R_0(R_{F1} - R_{F2})}{(2R_0 + R_{F2})(2R_0 + R_{F1})} \right), \qquad (34)$$

$$\Delta V = V_0 \frac{R_{F1} - R_{F2}}{4R_0 + 2(R_{F2} + R_{F1}) + R_{F1}R_{F2}/R_0}. \qquad (35)$$

Equation (35) describes the relation between the output measured voltage, ΔV, and the output torque, $\tau = f(\Delta V)$. Assuming the following assumption:

$$4R_0 \gg 2(R_{F2} + R_{F1}) + R_{F1}R_{F2}/R_0. \qquad (36)$$

Equation (18) become as following:

$$\Delta V_a = V_0 \frac{(R_{F1} - R_{F2})}{4R_0}, \qquad (37)$$

where ΔV_a is an approximation of the real value. The equation (37) represents an error in the measurement. From equation (36), this error is maximal when $R_{F2} \approx R_{F1}$, although, the equation $\Delta V \approx 0$, therefore this condition is not considered as an issue, since the output torque is negligible. The risk condition is when the output torque is higher, therefore, either $R_{F1} = 0$ or $R_{F2} = 0$. Assuming $R_{F1} = 0$, the equation (35) become as following:

$$\Delta V = -V_0 \frac{R_{F2}}{(4R_0 + 2R_{F2})} \qquad (38)$$

and what we approximate is as following:

$$\Delta V_a = -V_0 \frac{R_{F2}}{4R_0}. \qquad (39)$$

Equation (39) shows that by using this voltage driver configuration (figure 6(b)) the range of output is half with the previous configuration (figure 6(a)), showed in equation (28).

The error in the measurement is represented by the following equation:

$$e = \frac{\Delta V - \Delta V_a}{\Delta V} \qquad (40)$$

and by using the equations (39) and (40), the error is as following:

$$e = 1 - \frac{4R_0 + 2R_{F2}}{4R_0} = -\frac{R_{F2}}{2R_0} \qquad (41)$$

and, assuming that $R_{F2} = GR_0$, where G is the ration between R_{F2} and R_0, which is not more than 0.1, the error become as following:

$$|e| = |\frac{GR_0}{2R_0}| = \frac{G}{2} \qquad (42)$$

with the value of 0.05, therefore 5.0% of maximal error. The measured error in this configuration (figure 6(b)), is two times larger than the previous one (figure 6(a)).

Configuration (c)

The solution shown in figure 6(c), proposes to use only two SGs and one A/D converter, simplifying the number of wires and electrical components.

The equation that describes the output is the following:

$$V = \frac{R_0 + R_{F2}}{(R_0 + R_{F1}) + (R_0 + R_{F2})}, \qquad (43)$$

$$V = \frac{R_0 + R_{F2}}{2R_0 + R_{F1} + R_{F2}} \qquad (44)$$

by adding and subtracting the same quantity, $R_0 + R_{F1}$, the equation become as following:

$$V = \frac{R_0 + R_{F2} + R_0 + R_{F1} - R_0 - R_{F1}}{2R_0 + R_{F1} + R_{F2}} \qquad (45)$$

$$= \frac{(2R_0 + R_{F2} + R_{F1}) - (R_0 + R_{F1})}{2R_0 + R_{F1} + R_{F2}} \tag{46}$$

$$= 1 - \frac{R_0 + R_{F1}}{2R_0 + R_{F1} + R_{F2}}. \tag{47}$$

By using the equation (22), R_{F2} can be represented by the following equations:

$$\Delta R_F = R_{F2} - R_{F1}, \tag{48}$$

$$R_{F2} = \Delta R_F + R_{F1}. \tag{49}$$

By using the previous representation, the equation (47) become as following:

$$V = 1 - \frac{R_0 + R_{F1}}{2R_0 + 2R_{F1} + \Delta R_F} \tag{50}$$

$$= 1 - \frac{1}{2 + \frac{\Delta R_F}{R_0 + R_{F1}}}. \tag{51}$$

The equation has two variables to be defined therefore cannot be solved. In order to simplify the problem, can be considered that in MiRA, one SMA provide a force that is much higher than the other, therefore the system can be in either $R_{F1} \gg R_{F2}$ or $R_{F2} \gg R_{F1}$, because does not make so much sense to active both at the same time with an high force, since the output torque will be negligible. Assuming this circumstance, the equation (51) can have the following solutions.

Condition (i) where $R_{F1} \gg R_{F2}$:

$$V = 1 - \frac{1}{2 - \frac{R_{F1}}{R_0 + R_{F1}}}. \tag{52}$$

Condition (ii) where $R_{F2} \gg R_{F1}$:

$$V = 1 - \frac{1}{2 + \frac{R_{F2}}{R_0}}, \tag{53}$$

where is evident that the condition (i) has a wider range than condition (ii), therefore F_1 output resolution is higher than F_2.

As in the previous configuration, the error is related to the ration between F_1 and F_2.

References

[1] Hu H, Wang P, Zhao B, Li M and Sun L 2009 Design of a novel snake-like robotic colonoscope *2009 IEEE Int. Conf. on Robotics and Biomimetics (ROBIO)* pp 1957–61

[2] Ma J, Li Y and Ge S 2012 Adaptive control for a cable driven robot arm *2012 Int. Conf. on Mechatronics and Automation (ICMA)* pp 1074–9

[3] Piccigallo M, Scarfogliero U, Quaglia C, Petroni G, Valdastri P, Menciassi A and Dario P 2010 Design of a novel bimanual robotic system for single-port laparoscopy *IEEE/ASME Trans. Mechatronics* **15** 871–8

[4] Robinson G and Davies J 1999 Continuum robots—a state of the art *1999 Proc., 1999 IEEE Int. Conf. on Robotics and Automation* vol 4 pp 2849–54

[5] Aral F, Azuma D, Narumi K, Yamanishi Y and Lin Y-C 2007 Design and fabrication of a shape memory alloy actuated exoskeletal microarm *2007 Int. Symp. on Micro-NanoMechatronics and Human Science MHS '07* pp 339–43

[6] Peirs J, Reynaerts D, Brussel H V, Gersem G D and Tang H-W 2003 Design of an advanced tool guiding system for robotic surgery *Proc. 2003 IEEE Int. Conf. on Robotics and Automation, ICRA 2003* vol 2 *(Taipei, Taiwan, 14–19 September, 2003)* (IEEE) pp 2651–6

[7] Simaan N, Taylor R and Flint P 2004 High dexterity snake-like robotic slaves for minimally invasive telesurgery of the upper airway *Medical Image Computing and Computer-Assisted Intervention â MICCAI 2004* (ser. *Lecture Notes in Computer Science* 3217) ed C Barillot *et al* (Berlin: Springer) pp 17–24

[8] Lam T L and Xu Y 2011 A flexible tree climbing robot: Treebot—design and implementation *2011 IEEE Int. Conf. on Robotics and Automation (ICRA)* pp 5849–54

[9] Moses M, Kutzer M, Ma H and Armand M 2013 A continuum manipulator made of interlocking fibers *IEEE Int. Conf. on Robotics and Automation (ICRA)* doi: 10.1109/ICRA.2013.6631142

[10] Kim Y-J, Cheng S, Kim S and Iagnemma K 2013 A novel layer jamming mechanism with tunable stiffness capability for minimally invasive surgery *IEEE Trans. Robot.* **29** 1031–41

[11] Yong-Jae Kim S K K I and Cheng S 2014 A stiffness-adjustable hyperredundant manipulator using a variable neutral-line mechanism for minimally invasive surgery *IEEE Trans. Robot.* **30** 382–95

[12] Ranzani T, Cianchetti M, Gerboni G, Falco I D and Menciassi A 2016 A soft modular manipulator for minimally invasive surgery: design and characterization of a single module *IEEE Trans. Robot.* **32** 187–200

[13] Cestari M, Sanz-Merodio D, Arevalo J C and Garcia E 2015 An adjustable compliant joint for lower-limb exoskeletons *IEEE/ASME Trans. Mechatronics* **20** 889–98

[14] Yu H, Huang S, Chen G, Pan Y and Guo Z 2015 Human-robot interaction control of rehabilitation robots with series elastic actuators *IEEE Trans. Robot.* **31** 1089–100

[15] Abry F, Brun X, Sesmat S, Bideaux E and Ducat C 2015 Electropneumatic cylinder backstepping position controller design with real-time closed-loop stiffness and damping tuning *IEEE Trans. Control Syst. Technol.* **24** 541–52

[16] Torrealba R R and Udelman S B 2016 Design of cam shape for maximum stiffness variability on a novel compliant actuator using differential evolution *Mech. Mach. Theory* **95** 114–24

[17] Kani M H H, Bonabi H A Y, Bidgoly H J, Yazdanpanah M J and Ahmadabadi M N 2016 Design and implementation of a distributed variable impedance actuator using parallel linear springs *J. Mech. Robot.* **8** 021024

[18] Guo J and Tian G 2015 Conceptual design and analysis of four types of variable stiffness actuators based on spring pretension *Int. J. Adv. Robot. Syst.* **12** 5

[19] Jafari A, Tsagarakis N G and Caldwell D G 2011 Awas-ii: a new actuator with adjustable stiffness based on the novel principle of adaptable pivot point and variable lever ratio *2011 IEEE Int. Conf. on Robotics and Automation (ICRA)* pp 4638–43

[20] Jafari A, Vu H Q and Iida F 2015 Determinants for stiffness adjustment mechanisms *J. Intell. Robot. Syst.* **82** 435–54

[21] Jeong H, Cheong J and Kwon S 2015 Dual-mode variable stiffness actuator using two-stage worm gear transmission for safe robotic manipulators *Int. J. Precis. Eng. Manuf.* **16** 1761–9

[22] Mahvash M and Dupont P E 2011 Stiffness control of surgical continuum manipulators *IEEE Trans. Robot.* **27** 334–45

[23] Churchill C, Shaw J and Iadicola M 2009 Tips and tricks for characterizing shape memory alloy wire: II. Fundamental isothermal responses *Exp. Tech.* **33** 51–62

[24] Zhang X Y and Yan X J 2012 Continuous rotary motor actuated by multiple segments of shape memory alloy wires *J. Mater. Eng. Perform.* **21** 2643–9

[25] Leng J, Yan X, Zhang X, Huang D and Gao Z 2016 Design of a novel flexible shape memory alloy actuator with multilayer tubular structure for easy integration into a confined space *Smart Mater. Struct.* **25** 025007

[26] Zhang X, Wang S, Yan X, Yue D, Sun R and Zhou X 2016 Probabilistic analysis for the functional and structural fatigue of niti wires *Mater. Des.* **102** 213–24

[27] Cui D, Song G and Li H 2010 Modeling of the electrical resistance of shape memory alloy wires *Smart Mater. Struct.* **19** 055019

[28] Georges T, Brailovski V and Terriault P 2012 Characterization and design of antagonistic shape memory alloy actuators *Smart Mater. Struct.* **21** 035010

[29] Gilardi G, Haslam E, Bundhoo V and Park E j 2010 A shape memory alloy based tendon-driven actuation system for biomimetic artificial fingers: II. Modelling and control *Robotica* **28** 675–87

[30] Cuellar W C, Rossi C, Montaño J C and Cruz A B 2012 SMA-based muscle-like actuation in biologically inspired robots: a state of the art review *Smart Actuation and Sensing Systems? Recent Advances and Future Challenges* ed G Berselli *et al* (Rijeka: InTech)

[31] Spaggiari A, Mammano G S and Dragoni E 2012 *Smart Actuation and Sensing Systems—Recent Advances and Future Challenges* ed G Berselli (Rijeka: InTech)

[32] Huang S, Leary M, Ataalla T, Probst K and Subic A 2012 Optimisation of niti shape memory alloy response time by transient heat transfer analysis *Mater. Des.* **35** 655–63

[33] Ko J, Jun M B, Gilardi G, Haslam E and Park E J 2011 Fuzzy PWM-PID control of cocontracting antagonistic shape memory alloy muscle pairs in an artificial finger *Mechatronics* **21** 1190–202

[34] Kianzad S, Amini A and Karkouti S 2011 Force control of laparoscopy grasper using antagonistic shape memory alloy *2011 1st Middle East Conf. on Biomedical Engineering (MECBME)* pp 335–8

[35] Manfredi L, Velsink F, Khan H and Cuschieri A 2016 A variable impedance actuator based on shape memory alloy *Messe Bremen WFB Wirtschaftsförderung* ed H Borgmann (Bremen: GmbH) pp 167–70

[36] Mammano G S and Dragoni E 2011 Modeling of wire-on-drum shape memory actuators for linear and rotary motion *J. Intell. Mater. Syst. Struct.* **22** 1129–40

[37] Murata, http://murata.com

[38] Miyashita K, Takahashi T, Kawamata S, Morinaga S and Hoshi Y 1990 Noncontact magnetic torque sensor *IEEE Trans. Magn.* **26** 1560–2

[39] Lemarquand V and Lemarquand G 1995 Magnetic differential torque sensor *IEEE Trans. Magn.* **31** 3188–90

[40] Sasada I, Etoh Y and Kato K 2006 A figure-of-eight flexible pickup coil for a magnetostrictive torque sensor *IEEE Trans. Magn.* **42** 3309–11

[41] Wolffenbuttel R F and Foerster J A 1990 Noncontact capacitive torque sensor for use on a rotating axle *IEEE Trans. Instrum. Meas.* **39** 1008–13

[42] Myers D R and Pisano A P 2009 Torque measurements of an automotive halfshaft utilizing a mems resonant strain gauge *Transducers 2009-2009 Int. Solid-State Sensors, Actuators and Microsystems Conf.* pp 1726–9

[43] Lee S, Yang K, Shin E and Kim H 2014 Development of 1-axis torque sensor with different shape of support and measurement spoke *2014 11th Int. Conf. on Ubiquitous Robots and Ambient Intelligence (URAI)* pp 688–91

[44] Taghirad H D and Belanger P R 1999 Intelligent built-in torque sensor for harmonic drive systems *IEEE Trans. Instrum. Meas.* **48** 1201–7

[45] Aghili F, Buehler M and Hollerbach J M 2001 Design of a hollow hexaform torque sensor for robot joints *Int. J. Robot. Res.* **20** 967–76

[46] Hong D H, Kim Y G, Kwak J H, Jeong C P and An J 2012 Miniature force-torque sensor using semiconductor strain gage sensor frame design and analysis for development *2012 9th Int. Conf. on Ubiquitous Robots and Ambient Intelligence (URAI)* pp 627–8

[47] Liu S-H, Huang T-S and Yen J-Y 2010 Tracking control of shape-memory-alloy actuators based on self-sensing feedback and inverse hysteresis compensation *Sensors* **10** 112

[48] Micron instruments, http://microninstruments.com